

Journal of Materials Chemistry B

Accepted Manuscript



This is an *Accepted Manuscript*, which has been through the Royal Society of Chemistry peer review process and has been accepted for publication.

Accepted Manuscripts are published online shortly after acceptance, before technical editing, formatting and proof reading. Using this free service, authors can make their results available to the community, in citable form, before we publish the edited article. We will replace this *Accepted Manuscript* with the edited and formatted *Advance Article* as soon as it is available.

You can find more information about *Accepted Manuscripts* in the [Information for Authors](#).

Please note that technical editing may introduce minor changes to the text and/or graphics, which may alter content. The journal's standard [Terms & Conditions](#) and the [Ethical guidelines](#) still apply. In no event shall the Royal Society of Chemistry be held responsible for any errors or omissions in this *Accepted Manuscript* or any consequences arising from the use of any information it contains.

ARTICLE

Direct observation of the nanocomplex surface reorganization of antifouling silicones containing a highly mobile PEO-silane amphiphile

Cite this: DOI: 10.1039/x0xx00000x

Received 00th January 2012,
Accepted 00th January 2012

DOI: 10.1039/x0xx00000x

www.rsc.org/

Melissa L. Hawkins,^a Marc A. Rufin,^a Jefferey E. Raymond,^{*b} and Melissa A. Grunlan^{*a}

While nanocomplexity derived from surface reorganization in aqueous biofouling environments is known to give rise to antifouling behavior, quantification of this process is limited. In this work, the surface of an antifouling polymer matrix – a silicone modified with a highly mobile PEO-silane amphiphile – was characterized while undergoing dynamic surface reorganization in aqueous solution *via* off-resonance tapping mode atomic force microscopy (AFM) while monitoring surface changes at a rate $>25 \mu\text{m}^2/\text{min}$. Utilizing multimodal analysis during incubation in aqueous solution and surface force spectroscopic mapping before and after incubation, we directly observed the nanoscopically complex surface of the matrix and its five distinct stages of surface reorganization. Pre- and post-incubation nanomechanical mapping revealed a marked increase in Young's modulus and surface area, as well as increased adhesion and dissipative properties for the post-incubated surface. The observed topographic and viscoelastic changes are explained in terms of surface-air and surface-water interactions. These findings are compared to the bulk matrix reordering observed by immersion dynamic mechanical analysis (DMA) and enhanced protein resistance with increased submersion times as determined by confocal microscopy.

Introduction

Nanocomplex surfaces with exceptional antifouling behavior are of tremendous interest for medical, marine and industrial applications.¹⁻³ Surface nanocomplexity includes nanoscale variations in chemical composition, topography, modulus and viscoelasticity.^{4, 5} Amphiphilic polymeric materials, comprised of both hydrophobic and hydrophilic components, typically achieve surface nanocomplexity via surface restructuring upon exposure to an aqueous environment.⁶⁻⁸ Since biofouling occurs in aqueous environments, water-driven surface reorganization to form a nanocomplex surface is ideal. The kinetics of surface reorganization as well as the specific features of surface nanocomplexity are influenced by the nature of the amphiphilic polymer. Thus, towards the goal of improving antifouling behavior, the chemical and structural features of the amphiphilic polymer can be tuned. However, the direct measurement of the surface reorganization kinetics and surface nanocomplexity have received limited attention.⁹ As such, the ability to rationally design amphiphilic polymeric materials having superior antifouling behavior is limited.

Silicones, particularly silica-reinforced crosslinked polydimethylsiloxane (PDMS), are widely used to create devices and coatings for a host of applications. These include blood-contacting medical devices (e.g. hemodialysis catheters and cardiac pacing leads),¹⁰⁻¹² marine coatings¹³ and filtration membranes.¹⁴ However, due to their extreme hydrophobicity, silicones exhibit poor antifouling behavior.¹⁵⁻²⁰ Poly(ethylene

oxide) (PEO; or poly(ethylene glycol) (PEG)) is a neutral, hydrophilic polymer and exhibits high resistance to protein adsorption.^{16, 19, 21, 22} Thus, PEO, particularly in the form of crosslinkable PEO-silanes, have been incorporated into silicones via bulk crosslinking.²³⁻²⁷ For instance, PEO was introduced into silicones via the condensation crosslinking of triethoxysilylpropyl PEO monomethyl ether [(RO)₃Si(CH₂)₃-(OCH₂CH₂)_n-OCH₃] with α,ω -bis(Si-OH)PDMS.^{25, 26} In our recent work, we reported the introduction of a new "PEO-silane amphiphile" [α -(EtO)₃Si-(CH₂)₂-oligodimethylsiloxane₁₃-block-(OCH₂CH₂)₈-OCH₃] to a silica-reinforced silicone (Fig. 1).²⁷ As noted above, conventional PEO-silanes consist of a PEO segment connected to a crosslinkable end group by a short alkane spacer (e.g. propyl). In contrast, this PEO-silane amphiphile contains a flexible siloxane tether as the spacer. The flexibility of the siloxane tether is due to the wide bond angle ($\sim 145^\circ$) and low barrier to linearization (~ 0.3 kcal/mol) of Si-O-Si in dimethylsiloxanes.^{28, 29} The protein-resistant nature of PEO is attributed to its hydrophilicity and hydration³⁰ as well as its configurational mobility which produces an "exclusion effect" and an entropic penalty if adsorption were to occur.^{16, 19, 22, 31, 32} Thus, a flexible siloxane tether (rather than a short alkane spacer) should lead to enhanced PEO configurational

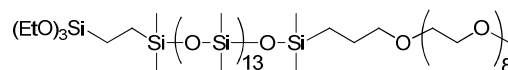


Fig. 1 Structure of PEO-silane amphiphile.

mobility. In addition, the siloxane tether is hydrophobic thereby creating a PEO-silane with amphiphilic character. Notably, when the PEO-silane amphiphile was introduced into the silicone (particularly at ≥ 5 wt%), a dramatic reduction in the adhesion of proteins was observed.²⁷ Temporal contact angle measurements of coatings indicated rapid migration of PEO chains to the water interface. For instance, with 10 wt% PEO-silane amphiphile added to the coating (~ 0.15 mm thick), contact angles ($^\circ$) were: 61.7 ± 1.1 (15 sec) $> 43.9 \pm 0.2$ (1 min) $> 33.4 \pm 0.1$ (2 min). Interestingly, similar spin-coated films (even with higher levels of PEG-silane amphiphile) exhibited diminished restructuring for thicknesses below ~ 0.5 μm (see Table S1). When the ~ 0.15 mm thick coatings were equilibrated in water just prior to analysis, rapid restructuring was likewise observed based on measured contact angles ($^\circ$): 89.6 ± 2.0 (15 sec) $> 54.7 \pm 1.4$ (1 min) $> 45.8 \pm 1.1$ (2 min). The unexpected higher contact angle values for the “water equilibrated coating” were explained based on the gravimetrically determined uptake of a small percentage of water (3.65%). It was rationalized that, upon absorption of water, some PEO re-entered the bulk. Still remaining is a quantitative assessment of the kinetics of surface reconstruction as well as the specific features of nanocomplexity thereby limiting our understanding of this antifouling coating system.

In this work, the aforementioned coating system, comprised of a silica-filled silicone matrix and PEO-silane amphiphile (10 wt%), was exposed to sequential aqueous submersion and drying while simultaneously being subjected to off-resonance tapping mode atomic force microscopy (AFM). Surface changes to the nanoscale viscoelastic and topographical properties were captured pre- and post-incubation in PBS using surface force spectroscopy (SFS). Restructuring kinetics were captured in an aqueous environment by off-resonance AFM at a rate > 25 $\mu\text{m}^2/\text{min}$. Multimodal analyses of the off-resonance AFM spectra were used to extract the kinetics for all experiments. Immersion dynamic mechanical analysis (DMA) was used to determine any interrelationship of bulk mechanical properties and surface restructuring. Protein adsorption was studied as a function of prior incubation time in PBS.

Experimental

Materials

Sodium bicarbonate and ACS-grade solvents were obtained from Sigma-Aldrich. Phosphate buffered saline (PBS, HyClone without calcium and magnesium, pH = 7.1) was obtained from Thermo Scientific. Glass microscope slides (75 x 50 mm; cut to a final size of 37.5 x 50 mm) were obtained from Fisher Scientific. Medical-grade silicone (MED-1137) was obtained from NuSil Technology (Carpinteria, CA). Per manufacturer specifications, MED-1137 is comprised of α,ω -bis(Si-OH)PDMS, silica (11–21%), methyltriacetoxysilane (<5%), ethyltriacetoxysilane (<5%) and trace amounts of acetic acid. The PEO-silane amphiphile [α -(EtO)₃Si(CH₂)₂-oligodimethylsiloxane₁₃-block-(OCH₂CH₂)₈-OCH₃] was prepared as previously reported.^{24, 27} Polished discs (18 mm diameter) were obtained from Ted Pella Inc. The Alexa Fluor 555-dye conjugate of bovine serum albumin (AF-555 BSA; MW = 66 kDa; lyophilized powder; > 96% BSA) and the Alexa Fluor 546-dye conjugate of human fibrinogen (AF-546 HF; MW = 340 kDa; lyophilized powder; 95% clottable protein) were purchased from Invitrogen (Carlsbad, CA).

Preparation of coated steel discs

The steel discs were sequentially washed with acetone, dichloromethane and acetone and dried in air at RT for 1 hr prior to use. In a scintillation vial, MED-1137 was combined with hexane (1:3, wt/wt) and the PEO-silane amphiphile (10 wt% based on MED-1137 wt). The sealed vial was placed on a shaker table for 4 hr to achieve a homogeneous solution. The solution was solvent-cast onto level metal discs (10 drops, 0.2 mL) and a polystyrene Petri dish cover placed on top. In this way, solvent evaporation was slowed which prevented the formation of gas bubbles in the coating. Coatings (~ 0.15 mm thick) were cured for 7 days at room temperature (RT).

Preparation of free-standing films for DMA and protein tests

MED-1137 was combined with hexane and the PEO-silane amphiphile as above. The solution was poured into a polystyrene Petri dish (50 mL) and covered. Films were allowed to cure for 7 days at RT. Next, films were removed from the Petri dish and cut to specified dimensions for further testing. A silicone control was prepared by combining MED-1137 with hexane (1:2, wt/wt). After obtaining a homogeneous solution, the silicone solution was solvent-cast onto level glass microscope slides (2.5 mL per slide) and allowed to cure as above. The silicone films (~ 0.55 mm thick) were removed from the slides with a clean single-edge razor blade to obtain free-standing films used for DMA and protein adsorption measurements.

Surface nanomechanics in response to PBS exposure

The surfaces of coated steel discs were subjected to quantitative nanomechanical mapping via SFS in both a dry pre-incubation and a dry post-incubation state. Following measurements of the pre-incubation state, the surfaces were incubated in PBS in a fluid isolation chamber (Bruker) for 140 min, removed, rinsed three times with nanopure water, gently wicked dry and placed under a dry, filtered N₂ flow for 30 hr. The surfaces were once more subjected to SFS measurements in this final post-incubation state.

In situ surface reorganization kinetics

Off-resonance AFM (Bruker Multimode 8) was performed on the surface of a coated steel disc immediately following exposure to PBS in a fluid isolation chamber (Bruker). A total of 160 images with corresponding height and phase values were generated over 140 min of incubation.

Atomic force microscopy (AFM)

A Bruker Multimode 8 AFM was used for all SFS measurements and for imaging reorganization kinetics. Bruker Scanasyt-Fluid+ AFM tips (per manufacturer specifications: $k = 0.7$ N/m, 150 kHz, N₄Si₃) were used. The same tip was used for all incubation states to eliminate tip-to-tip variation in surface-tip interactions and variations in tip geometry.

SFS was performed as detailed and applied elsewhere.³³ Calibration was performed before all measurements with a PDMS standard of known surface modulus and confirmed independently via tip and deflection quantification as detailed elsewhere.³³ The tip was rinsed with nanopure water and dried under a flow of N₂ for 5 min before each measurement. Briefly, the Derjaguin-Muller-Toporov (DMT) model³⁴ was used to calculate the modulus from the slope of the linear portion of the post-contact approach force curve. Dissipation energy was

calculated from the difference in the work function of the linear portion of the post-contact force curve in approach and retraction. Adhesion force was calculated from the differential of the pre-surface contact in approach and retraction. Deformation after contact was maintained at a median of 6 nm for all SFS assessed surfaces.

For reorganization kinetics experiments, fast scan (>25 $\mu\text{m}^2/\text{min}$), solution phase tapping mode AFM was performed at the peak of an off-primary resonance peak at 24 kHz with no peak off-set, resulting in a low noise environment. Drive amplitude was set and maintained at a 200 mV operating voltage (compared to the more conventional 1 V), resulting in a low enough magnitude that amplitude differential becomes an excellent tool for monitoring tip viability and surface solvation. The instrument was isolated by use of a bungeed stone plate suspended from a tripod. During tapping mode operation, amplitude data were also captured and mapped. Median amplitude differential was monitored for tip fouling during imaging, and imaging was stopped before the change in amplitude reached 1% of the total applied amplitude. Thus, the distortion of kinetic data due to tip fouling was avoided.

Immersion dynamic mechanical analysis (DMA)

Mechanical analysis of free-standing films (7.5 x 5.5 x 0.55 mm) was performed by immersion DMA with a TT-DMA (Mettler-Toledo) operated in the tension mode with strain controlled dynamic loading at 2% deformation under a static ratio stress load of 1.5 times the dynamic load. Measurements occurred over a 15 hr period of immersion in PBS over one decade of frequencies (1 to 10 Hz).

Protein adsorption

The adsorption of the Alexa Fluor dye conjugates of bovine serum albumin (AF-555 BSA) and human fibrinogen (AF-546 HF) onto free-standing film surfaces was studied with confocal laser scanning microscopy (CLSM). Films (10 x 10 x 0.55 mm) were placed in individual wells of a 24-well plate. One silicone control and seven PEO-modified silicone films were analyzed for each AF-555 BSA and AF-546 HF. Each well was filled with 0.9 mL of PBS for varying amounts of time (0, 5, 10, 30, 60, 90 and 120 min) prior to the deposition of AF-555 BSA and AF-546 HF solutions. At the specified time, 0.1 mL of AF-555 BSA solution (1 mg/mL in PBS) or AF-546 HF solution (1 mg/mL) was added to achieve a final protein concentration of 0.1 mg/mL.^{23, 24, 35} (Note: Per manufacturer specifications, the AF-546 HF was first dissolved in 0.1 M NaHCO_3 to obtain a 1.5 mg/mL solution and was further diluted in PBS to obtain a final concentration of 1 mg/mL.) After each film was equilibrated in the protein solution for 2 hr in the dark, the film was removed and placed in a polystyrene Petri dish. Fresh PBS (1 mL) was applied to the film and removed after 5 min. This process was repeated for a total of three times. The films were then wicked dry and imaged.

Confocal laser scanning microscopy (CLSM)

A FluoView 1000 (Olympus) confocal laser scanning microscope was used to quantify protein adsorption levels using a 1 mW HeNe excitation source (543 nm) with a monochromator bandpass of 555 - 655 nm for collection at a photomultiplier tube (PMT). A 10X objective (UPLSAPO 10x, Olympus) was used for imaging to maximize collection volume. Three film regions were imaged for each sample, with

identical scan rates, detector voltages and excitation powers. The emission histograms were then combined and integrations referenced to the known fouling density of the air-equilibrated, unmodified silicone. The emission histograms were adjusted to account for the surface autofluorescence of non-fouled, non-chromophore exposed films under this excitation and collection regime.

Results and discussion

Surface nanomechanics pre- and post-incubation in PBS

Quantitative nanomechanical mapping of the coating surface was performed via SFS over 0.25 μm^2 (Fig. 2) and 25 μm^2 (see Fig. S1) before and after exposure to PBS (140 min) and subsequent drying, resulting in four scans total each for the pre- and post-incubation conditions. Evaluation of a smaller versus

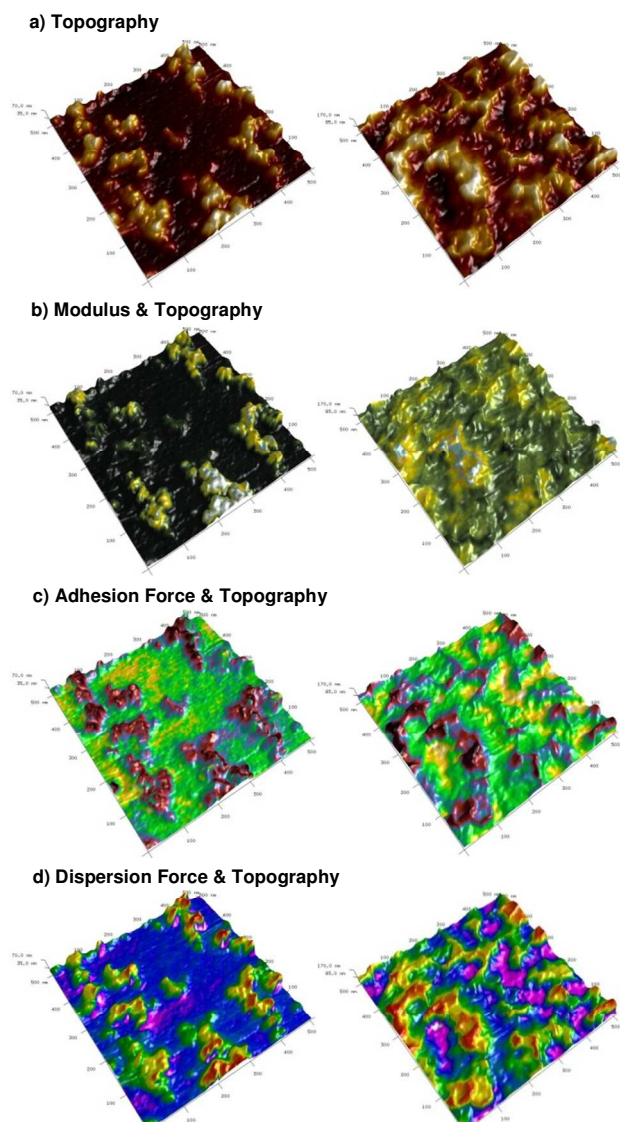


Fig. 2 SFS of a 0.25 μm^2 area before (left) and after (right) exposure to PBS; 500 x 500 nm^2 field of view. Displayed ranges are 0-60 nm, 0.1-2.5 MPa, 10-20 pN and 0-20 eV for the pre-incubation (left) and 0-140 nm, 4-11 MPa, 2.5-7.5 nN and 1-8 keV for the post-incubation (right) samples.

Table 1 Surface force spectral analysis

		0.25 μm^2		25 μm^2	
		Pre-	Post-	Pre-	Post-
Topography	ΔZ (nm)	64	160	130	190
	RMS _Z (nm)	10	30	18	24
	A (μm^2)	0.37	0.75	30.0	34.4
Modulus	E _{Young's} (MPa)	2.9	5.8	2.0	6.0
	RMS _E (MPa)	4.8	1.3	1.6	1.5
Adhesion Force	Force _{Adh} (nN)	-0*	5.5	0.18	7.0
	RMS _{Adh} (nN)	0.02	0.9	0.08	0.83
Dissipation	Dissipation (keV)	-0*	4.3	0.19	5.3
	RMS _{Dis} (keV)	0.03	1.8	0.5	1.5

RMS = root-mean-squared variation for each metric; A = surface area;
*spectra within error of zero.

larger area permitted capture of surface nano- and meso-scale heterogeneity. For all four scans, full field of view spectral analysis was performed and the results are presented in Table 1 as well as in histograms (Fig. 3). Surface images of nanoscale features in Fig. 2 are height projections with modulus, adhesion force and dispersion force spectra individually overlaid. Spectral maps are centered on the mean with a range of two standard deviations.

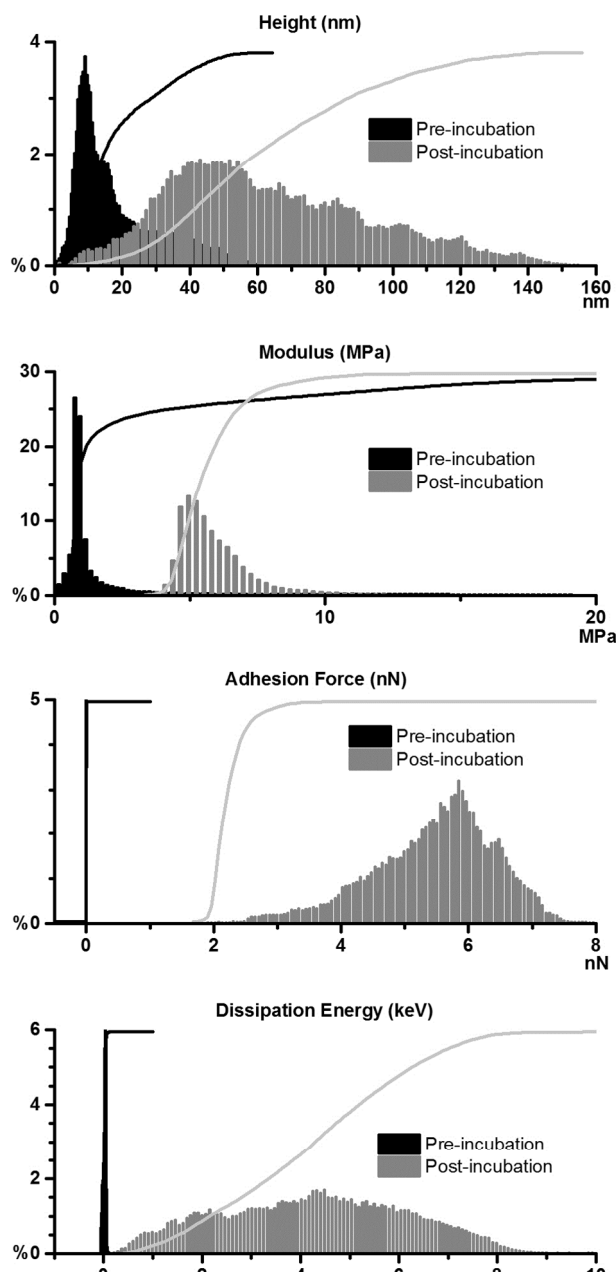
Topographic data (Table 1, Fig. 2a), including the total height differential (ΔZ), height root-mean-squared roughness (RMS_Z) and projected surface area (A), showed a gross increase in feature dimensions post-incubation. Most striking was a tripling of RMS_Z and a doubling of A across the 0.25 μm^2 surface, thus signifying a far more complicated surface landscape upon aqueous exposure. Similar trends were observed across the 25 μm^2 surface (Table 1, see Fig. S1).

The modulus (E_{Young's}) of the 0.25 μm^2 surface before and after PBS exposure displayed two trends which indicate stabilization of the post-incubated surface despite an increase in surface roughness (Table 1, Fig. 2b). First, E_{Young's} post-incubation doubled, a phenomenon reminiscent of solvent annealing. Second, post-incubation, the modulus variation (RMS_E) decreased to a third of the pre-incubation value. Combined, these observations indicate that the effects of water-surface interactions (i.e. surface restructuring) remain even following removal of the surface from PBS. Similar results were recorded for the 25 μm^2 surface (Table 1, see Fig. S1). Per Fig. 2b, for both pre- and post-incubated surfaces, high and low E_{Young's} regions are primarily associated with peaks and valleys in height, respectively. This consistency indicates that the basic surface heterogeneity is a result of comparable changes in both the E_{Young's} and topography. Finally, following PBS incubation, the increase in E_{Young's} values from ca. 2 MPa to ca. 6 MPa is consistent with the transition from a crosslinked silicone surface (see DMA results) to that of a densely packed plasticized PEO surface.³⁶

Adhesion force (Force_{Adh}) and dissipation were used to characterize the change in surface tackiness and mechanical lossiness, respectively (Table 1, Fig. 2c and 2d, see Fig. S1). The spectral maps display a pre-incubated surface with non-tip-adherent and non-dispersive character. Post-incubation, the surface is transformed into a highly adherent and dispersive surface. The increase in dissipation energy of the post-incubated surface signifies reduced restorative compression, further suggesting that the rubbery crosslinked silicone matrix

is relatively less present and PEO relatively more present after PBS exposure. Inspection of the overlaid maps of adhesion force and height (Fig. 2c) and of dispersion force and height (Fig. 2d) reveal that these features correspond with one another such that the more adherent and lossy features are located at the peaks in height.

Combining the information from topography, modulus, adhesion and dispersion measurements, differences between the pre- and post-incubation surface states emerge. Pre-incubation, the surface shows no expression of PEO-like character. The surface exhibits low surface roughness (i.e. low RMS_Z) while modulus variation (i.e. RMS_E) may be due to the heterogeneity of a silica-filled silicone component. Post-incubation, the underlying silica-filled silicone experiences an increase in E_{Young's} due to a solvent annealing-like effect. However, the

**Fig. 3** Surface force spectral mapping histograms.

thin, elevated layer is enriched with tip-adherent and dispersive PEO chains. This total change of surface state strongly supports the hypothesized reorganization of tethered PEO-silane amphiphile chains to the surface-water interface.

In situ surface reorganization kinetics

While the aforementioned SFS mapping and spectra provide valuable information about the pre- and post-incubation surface states, they provide little information about the rate and mechanism of this change of state due to PEO-silane amphiphile restructuring. In order to capture the reorganizational kinetics at the surface-water interface, off-resonance AFM was performed temporally on the surface immediately following submersion in PBS for 140 min. Select images of the surface reorganization (i.e. increasing roughness and arrival of large features) can be observed in Fig. 4 and as a 5 min/frame height movie (see ESI).

For full analysis of reorganization kinetics and relative differences in coating surface properties, the data must be extracted from each image. Thus, multiple whole-image signals were extracted from all 160 image arrays collected from AFM imaging. The metrics utilized for calculations include height and surface area (ΔZ ; A_{surf}), roughness (RMS_Z ; σ_Z), phase (ΔPh ; RMS_{Ph} ; σ_{Ph}) and amplitude (ΔAmp ; σ_{Amp}) (see Table S2). Temporal spectra (0 to 140 min) for each of these metrics are provided in Fig. 5a-d. While any of these metrics can be regionally fitted for reordering kinetics, each signal has its strengths and weaknesses in relation to tracking surface change. For example, phase contrast imaging alone is excellent for identifying boundaries (e.g. compositional gradients) but not for determining the magnitude of spatial reordering. Thus, a “composite signal” comprised of a normalized linear combination of ΔZ , A_{surf} , RMS_Z , ΔPh , RMS_{Ph} , and ΔAmp was generated and used for fitting. This composite spectrum is provided, with fitting curves and residuals, in Fig. 5e. Time constants of surface feature reorganization are detailed in Table 2. Temporal “regions” of reorganization kinetics are assigned as follows and the final state of each region is depicted in Fig. 6:

Region I – PEO-rich regions migrate towards the surface [minutes 0-12]. When exposed to PBS, a consolidation of surface features occurred whereby portions deeper within the coating surface emerged and approached the heights of pre-existing surface features. Notably, there was a decrease in height variation, surface area, roughness, phase variation and amplitude variation. This transition was assigned to the surface expression of PEO-rich regions that were previously excluded from the pre-incubated surface due to surface energy effects during cure in air. This process occurred quite rapidly, with a time constant ($\tau = 1$ min) only slightly longer than the temporal resolution of the spectra.

Region II – PEO-poor regions digress from the surface [minutes 12-18]. During this ‘cross-over’ period, the silicone matrix retracted such that PEO-rich regions passed PEO-poor regions in height (Z). The signals indicate a momentarily convoluted surface in which PEO-rich structures existed beneath PEO-poor structures and vice versa. This state was immediately followed by a return to a state similar to *Region I* in terms of roughness albeit with an overall greater surface area and phase variation. The final state of *Region II* was PEO-rich over a PEO-poor surface. This process was only marginally slower ($\tau = 2$ min) than that observed in *Region I*.

Region III – PEO-rich regions extend from the matrix [minutes 18-32]. This region marks the end of PEO migration

towards the surface and the onset of tall PEO-rich “nodes” (500 nm – 1 μm diameter). During this region, the surface area notably increased to its highest point for the entire experiment and height variation plateaued at ~ 600 nm. In addition, the amplitude variation spiked at the inflection point of feature

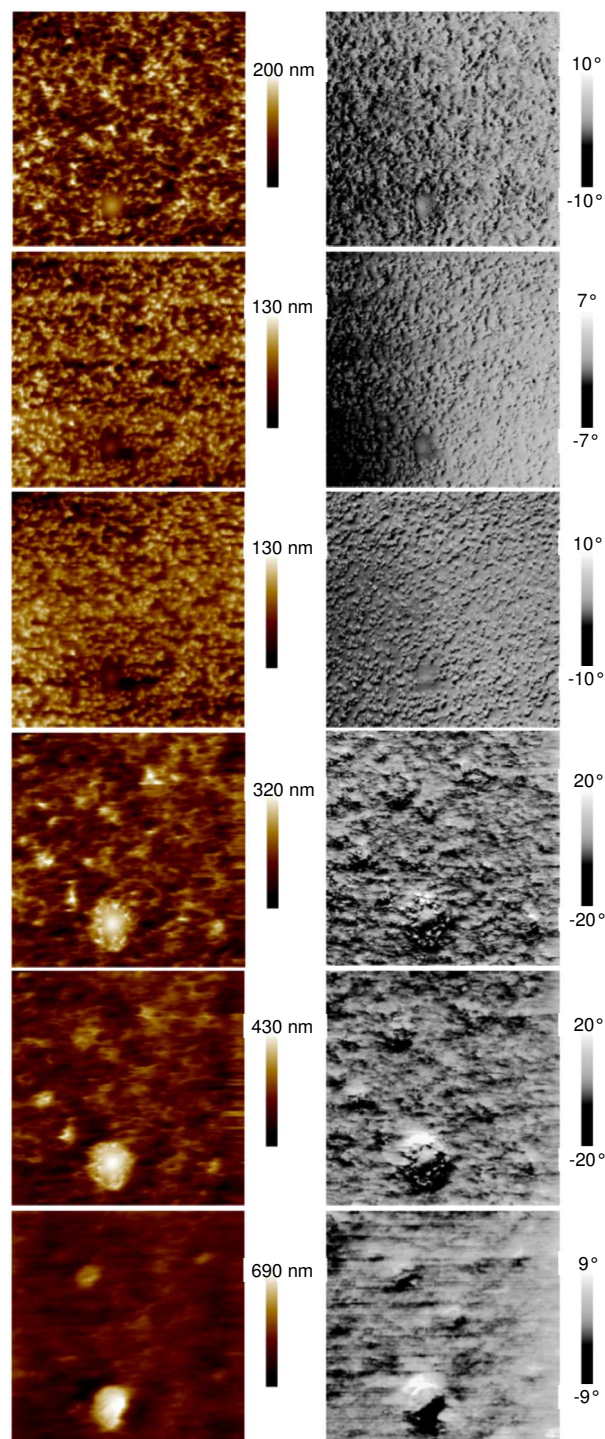


Fig. 4 Dynamic surface reorganization over 140 min. AFM height (left) and phase (right). Top to bottom: initial state, PEO expression towards surface at 10 min (*Region I*), PDMS recession into matrix at 15 min (*Region II*), PEO expression over surface at 30 min (*Region III*), PEO swelling at 60 min (*Region IV*) and solvation of tethered PEO ‘tails’ at 120 min (*Region V*).

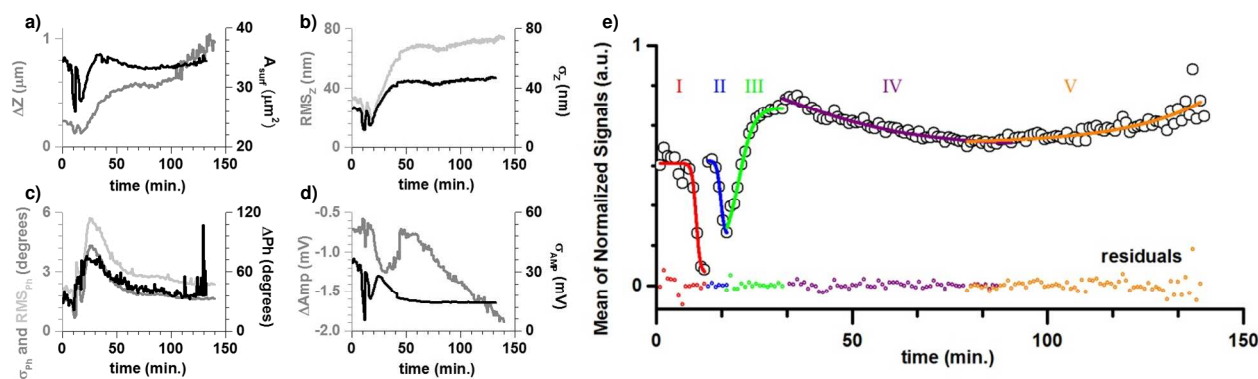


Fig. 5 Surface reorganization kinetics. (a) Height & surface area: ΔZ , A_{surf} ; (b) Roughness: RMS_Z , σ_Z ; (c) Phase: ΔPh , RMS_{Ph} , σ_{Ph} ; (d) Amplitude: ΔAmp , σ_{Amp} ; (e) Normalized mean of all extracted channels with annotated fitting and residuals.

Table 2 Time constants for surface reorganization

Region	Onset (min after t_0)	End (min after t_0)	τ (min)	$t_{1/2}$ (min)
I	7.6	12.3	1.0 ± 0.3	2.5
II	12.3	18.0	2.0 ± 0.4	3.9
III	18.0	32.2	5.2 ± 0.5	4.5
IV	32.2	87.0	27 ± 4	15.1
V	87.0	--	19 ± 5	--

Onset and end taken as inflection point for each region; τ = rate constant derived from exponential fitting of each region; $t_{1/2}$ = empirical midpoint of fitted region after onset.

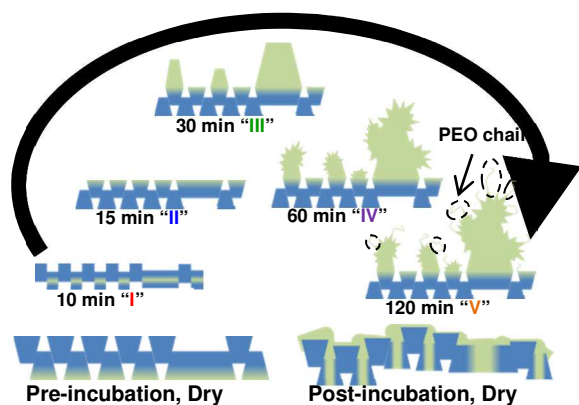


Fig. 6 Schematic depiction of final state of each temporal region I-V during *in situ* surface reorganization.

growth and decayed afterwards. This indicates a period in which the viscoelastic properties varied significantly followed by less variation in which the surface became more uniform in terms of tip-polymer interactions. This process, involving a large amount of PEO-rich material reorganizing to the surface collectively occurred more slowly ($\tau = 5$ min) than the processes of *Regions I* and *II* involving primarily the mobilization of PEO chains and smaller pockets of PEO-rich regions.

Region IV – Swelling of PEO-rich nodes [minutes 32-87]. During this region, the surface is consumed by the PEO-rich nodes that first appeared in *Region III*. This coincides with a small decrease in surface area a relatively constant roughness and a growing uniformity of phase profile with a decrease in

variation and total range. PEO-enriched domains underwent solvent-swelling and was significantly slower ($\tau = 27$ min) versus preceding regions. This solvation effect was more significant in the PEO-rich regions relative to the PEO-poor regions.

Region V – Solvation of PEO tails [minutes 87-140]. This final measured region is assigned to the maximization of hydrodynamic volume of PEO chains due to solvation. Sudden spikes in Z are observed over the larger features, producing a large ΔZ . Surface area and roughness began to increase again, with phase signals and amplitude variation all indicating a more uniform viscoelastic response across the entire surface. The most pointed manifestation of this process was observed in changes to the Z maxima. Changes in this region occurred faster ($\tau = 19$) than processes observed in *Region IV*. This is attributed to the fact that, during *Region IV*, much of the energy requirements for PEO tail-PEO tail dissociations had been met, in turn leaving a process more akin to the faster PEO-rich migrations observed in *Regions I* and *III*.

In conjunction with the post-incubated surface measured by SFS, these AFM results indicate that the residual polymer at the surface contributes to a gross increase of adhesion and dispersion and is most likely due to the PEO tails' lack of sufficient energetic incentive to return below the surface. Given that the entire surface appears to possess this quality, the post-incubated surface is assumed to be effectively fully PEO-enriched in terms of topography. Also of note, the overall increase in modulus can only be described as being induced by a solvent annealing-like effect, and not true solvent annealing, due to the observed adhesion and dispersion properties which indicate the absence of crystalline character. Enhanced surface homogeneity of the silicone matrix below a PEO-enriched layer is assumed, as a significant amount of the previous sub-surface amphiphile tethers are now on the surface, providing a less complex and mobile crosslinked network.

Bulk mechanical response

In order to observe any correlation between the bulk mechanical response of the system and the restructuring kinetics observed by AFM, DMA was performed at biologically relevant conditions (37 °C in PBS). Storage modulus (E') values over one decade of frequency (1 Hz to 10 Hz) displayed a linear increase over 15 hr (Fig. 7). Specifically, E' linearly increased by $7.03 \text{ kPa/h} \pm 0.05$ at 1 Hz while both loss modulus (E'') and $\tan \delta$ remain relatively flat. Changes in mechanokinetic response did not occur over this period, and specifically during the first 2 hr (coinciding to the observed

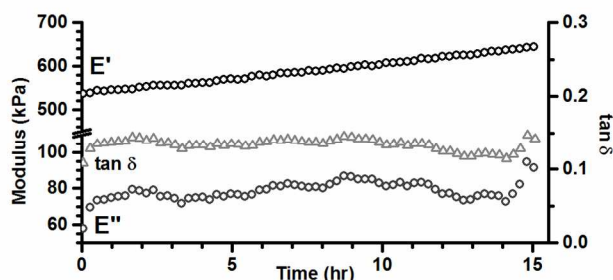


Fig. 7 Storage modulus (E'), $\tan \delta$ and loss modulus (E'') of the PEO-silane amphiphile modified silicone during 15 hours of incubation in PBS (37 °C).

incubation period as measured via AFM). Thus, the surface reorganization is not related to the bulk response of the matrix in any obvious fashion. The increase in E' from 540 kPa to 640 kPa implies matrix contraction for a plasticized system above its T_g or, in the case of a hydrophilically-modified (e.g. PEO) systems, a transition to a slightly swollen state with greater restorative response to stress. Since this coating displays low water uptake,²⁷ gradual contraction of the matrix assisted by a small amount of absorbed solvent intercalation into the silicone matrix reasonably accounts for the changes observed.

Protein adsorption

To observe how the surface restructuring observed by AFM relates to bulk antifouling response, the adsorption of BSA and HF was monitored as a function of incubation time in PBS (Fig. 8). Pre-incubation ($t = 0$), PEO-silane amphiphile modified silicone displayed *ca.* 5 and 4 times better resistance to BSA and HF, respectively, versus the unmodified silicone. Upon incubation in PBS, a marked increase in protein resistance was observed for the modified silicone (Fig. 8). In agreement with the rapid nature of PEO-silane amphiphile restructuring to the surface-water interface, protein adsorption decreased substantially at just $t = 5$ and 10 min of incubation. With 120 min of incubation time, a 77-fold increase in resistance to BSA and a 38-fold increase in resistance to HF were observed.

Conclusions

In this work, we present the water-driven surface reorganization kinetics of a nanoscopically complex antifouling surface

prepared by modification of silicone with a PEO-silane amphiphile containing a hydrophobic, flexible siloxane tether. While it is known that amphiphilic, nanocomplex surfaces reorder dynamically when exposed to an aqueous environment, previous studies have largely focused on spectroscopic, dynamic contact angle or initial versus final topographic states.^{5, 37} In this way, we reported herein the nanomechanical assessment of the surface before and after reorganization which revealed a post-incubation PEO-rich state where surface-reconstructed tethered PEO chain amphiphiles remain on the surface, providing both a higher modulus and greater dissipation. Moreover, these methods captured the topography-mechanical interplay at rates and scales appropriate for a heterogeneous nanocomplex surface. Moreover, reported here for the first time is the direct topographic observation of the temporal restructuring process of a surface comprised of amphiphiles in a silicone matrix when exposed to an aqueous environment. The restructuring consisted of five unique processes which began with the tethered PEO chain amphiphile largely embedded below the surface and ended with a final state where high solvent-PEO interaction volumes are obtained. These processes can be summarized as: (I) PEO-rich regions migrated towards the surface, (II) PEO-poor regions digressed from the surface, (III) PEO-rich nodes extended from the surface, (IV) PEO-rich nodes swelled, then began expressing (V) a canopy of hydrodynamically voluminous amphiphile PEO 'tails'. Notable was the rapid nature of these processes, particularly during I-III, which point to the high mobility of these PEO-silane amphiphiles imparted by their unique chemical structure. In addition, the increased protein resistance of the modified silicones after only brief periods of incubation ($t \leq 10$ min) and continued increase with extended incubation periods (up to 120 min) agree with the observed temporal changes of the reorganized surface. Thus, the reported analyses demonstrate a quantitative measure of the rate and extent of surface reconstruction in aqueous environments which can be used to better explain and understand the antifouling behavior. Moreover, the benefits of solvent (water) pre-conditioning to enhance antifouling behavior as well as to increase mechanical properties such as modulus and dissipation were captured.

Acknowledgements

The authors gratefully acknowledge funding support from the Texas Engineering and Experiment Station (TEES), the Office

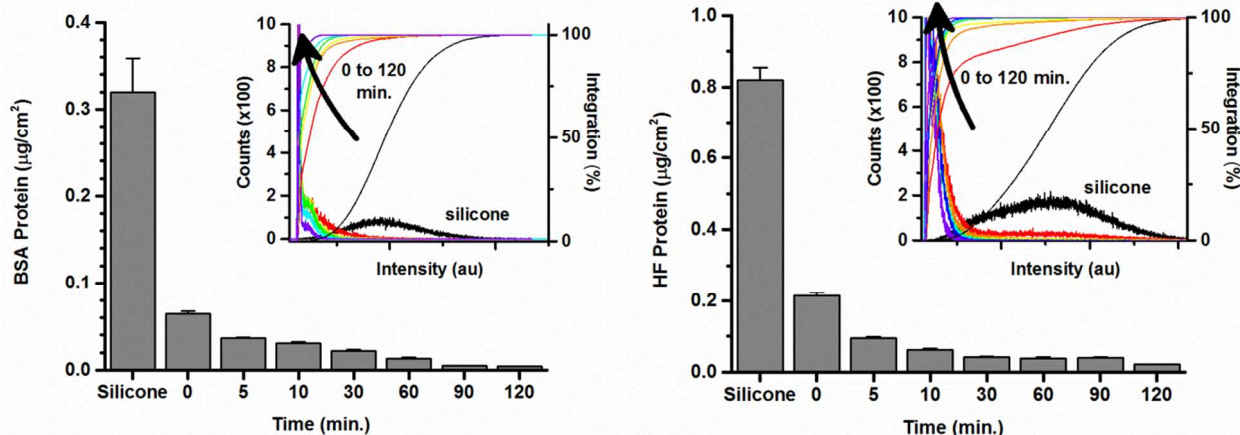


Fig. 8 Protein adsorption of the air-equilibrated silicone control and the PEO-silane amphiphile modified silicone as a function of PBS incubation time. (a) BSA and (b) HF adsorption with insets of fluorescence histograms and integrations.

of Naval Research (N00014-10-1-0527) and the Welch Foundation (A-001). M.L.H thanks the Texas A&M University Diversity Fellowship Program for support.

Notes and references

^a Texas A&M University, Department of Biomedical Engineering, Department of Materials Science and Engineering, 5030 Emerging Technologies Building, 3120 TAMU, College Station, United States. Fax: 979 845 4450; Tel: 979 845 5532; E-mail: mgrunlan@tamu.edu

^b Texas A&M University, Department of Chemistry, Laboratory for Synthetic-Biologic Interactions, 1030 Chemistry, 3255 TAMU, College Station, United States. Fax: 979 862 3714; Tel: 979 862 3713; E-mail: jefferey.raymond@chem.tamu.edu

† Electronic Supplementary Information (ESI) available: Large field-of-view (25 μm^2) SFS maps (Fig. S1), contact angle analysis of spin-coated films (Table S1), metrics of reorganization kinetics (Table S2), and reorganization movie at 5 min/frame. See DOI: 10.1039/b000000x/

- S. Dobretsov, A. M. Romaní, D. A. Spratt, D. Ready and J. Pratten, in *Biofouling*, eds. S. Dürr and J. C. Thomason, Wiley-Blackwell, 2010, pp. 121-122.
- R. Edyvean, in *Biofouling*, eds. S. Dürr and J. C. Thomason, Wiley-Blackwell, 2010, pp. 217-225.
- M. P. Schultz, K. A. Bendick, E. R. Holm and W. M. Hertel, *Biofouling*, 2011, **27**, 87-98.
- D. Gan, A. Mueller and K. L. Wooley, *J. Polym. Sci., Part A: Polym. Chem.*, 2003, **41**, 3531-3540.
- P. M. Imbesi, J. A. Finlay, N. Aldred, M. J. Eller, S. E. Felder, K. A. Pollack, A. T. Lonacker, J. E. Raymond, M. E. Mackay, E. A. Schweikert, A. S. Clare, J. A. Callow, M. E. Callow and K. L. Wooley, *Polym. Chem.*, 2012, **3**, 3121-3131.
- S. Krishnan, N. Wang, C. Ober, J. Finlay, M. Callow, J. Callow and D. Fischer, *Langmuir*, 2006, **22**, 5075-5086.
- E. Martinelli, S. Agostini, G. Galli, E. Chiellini, A. Glisenti, M. Pettitt, M. Callow, J. Callow, K. Graf and F. Bartels, *Langmuir*, 2008, **24**, 13138-13147.
- D. Park, C. Weinman, J. Finlay, B. Fletcher, M. Paik, H. Sundaram, M. Dimitriou, K. Sohn, M. Callow and J. Callow, *Langmuir*, 2010, **26**, 9772-9781.
- C. M. Kirschner and A. B. Brennan, *Annu. Rev. Mater. Res.*, 2012, **42**, 211-229.
- J. Curtis and A. Colas, in *Biomaterials Science: An Introduction to Materials in Medicine*, eds. B. D. Ratner, A. S. Hoffman, F. J. Schoen and J. E. Lemons, Elsevier Academic Press, San Diego, CA, 2nd edn., 2004, pp. 697-707.
- M. E. VanDyke, S. J. Clarson and R. Arshady, in *An Introduction to Polymeric Biomaterials*, ed. R. Arshady, Citrus Books, London, 2003, vol. 1, pp. 109-135.
- H. S. El-Zaim and J. P. Heggors, in *Polymeric Biomaterials, 2nd Edition*, ed. S. Dumitriu, Marcel Dekker, Inc., New York, NY, 2002, pp. 79-90.
- M. Lejars, A. Marigaillan and C. Bressy, *Chemical Rev.*, 2012, **112**, 4347-4390.
- T. A. Desai, D. J. Hansford, L. Leoni, M. Essenpreis and M. Ferrari, *Biosens. Bioelectron.*, 2000, **15**, 453-462.
- S. Krishnan, C. J. Weinman and C. K. Ober, *J Mater Chem*, 2008, **18**, 3405-3413.
- S. I. Jeon, J. H. Lee, J. D. Andrade and P. G. DeGennes, *J. Colloid Interf. Sci.*, 1991, **142**, 149-158.
- V. Bartzoka, M. R. McDermott and M. A. Brook, *Adv. Mater.*, 1999, **11**, 257-259.
- P. Hron, *Polym. Int.*, 2003, **52**, 1531-1539.
- S. I. Jeon, J. H. Lee, J. D. Andrade and P. G. DeGennes, *J Colloid Interf Sci*, 1991, **142**, 149-158.
- J. M. Anderson, N. P. Ziats, A. Azeez, M. R. Brunstedt, S. Stack and T. L. Bonfield, *J. Biomater. Sci. Polym. Ed.*, 1995, **7**, 159-169.
- W. R. Gombotz, W. Guanghui, T. A. Horbett and A. S. Hoffman, *J Biomed Mater Res*, 1991, **25**, 1547-1562.
- J. H. Lee, H. B. Lee and J. D. Andrade, *Prog Polym Sci*, 1995, **20**, 1043-1079.
- R. Murthy, B. M. Bailey, C. Valentin-Rodriguez, A. Ivanisevic and M. A. Grunlan, *J. Polym. Sci. Part A: Polym. Chem.*, 2010, **48**, 4108-4119.
- R. Murthy, C. D. Cox, M. S. Hahn and M. A. Grunlan, *Biomacromolecules*, 2007, **8**, 3244-3252.
- H. Chen, M. A. Brook, Y. Chen and H. Sheardown, *J. Biomater. Sci. Polym. Ed.*, 2005, **16**, 531-548.
- H. Chen, M. A. Brook and H. Sheardown, *Biomaterials*, 2004, **25**, 2273-2282.
- M. L. Hawkins and M. A. Grunlan, *J. Mater. Chem.*, 2012, **22**, 19540-19546.
- J. E. Mark, in *Silicon-based polymer science: a comprehensive resource. Advances in chemistry series*, eds. J. M. Zeigler and F. W. G. Fearon, American Chemical Society, Washington, D. C., 1990, vol. 224.
- T. H. Lane and S. A. Burns, in *Immunology of silicones*, eds. M. Potter and N. R. Rose, Springer, Berlin, 1996.
- D. L. Elbert and J. A. Hubbell, *Annu. Rev. Mater. Sci.*, 1996, **26**, 365-394.
- D. Knoll and J. Hermans, *J. Biol. Chem.*, 1983, **258**, 5710-5715.
- E. Oesterberg, K. Bergstroem, K. Holmberg, J. A. Riggs, J. M. VanAlstine, T. P. Schuman, N. L. Burns and J. M. Harris, *Colloid Surface A*, 1993, **77**, 159-169.
- P. M. Imbesi, J. E. Raymond, B. S. Tucker and K. L. Wooley, *J. Mater. Chem.*, 2012, **22**, 19462-19473.
- B. V. Derjaguin, V. M. Muller and Y. P. Toporov, *J. Colloid Interf. Sci.*, 1975, **53**, 314-326.
- R. Murthy, C. E. Shell and M. A. Grunlan, *Biomaterials*, 2009, **30**, 2433-2439.
- S. A. Soule and K. V. Cashman, *J. Volcanol. Geoth. Res.*, 2004, **129**, 139-153.
- P. M. Imbesi, C. Fidge, J. E. Raymond, S. I. Cauët and K. L. Wooley, *ACS Macro Lett.*, 2012, **1**, 473-477.

The water-driven, dynamic nanoscale reorganization of PEO-silane amphiphiles within a silicone matrix was directly observed via atomic force microscopy.

